# High Resolution Cross Well Imaging of a West Texas Carbonate Reservoir: Part 4. Reflection Imaging

BG1.5

*S. K. Lazaratos*, J. M. Harris, Stanford Univ.; J. W. Rector III, Univ. of California, Berkeley (formerly Stanford Univ.); and M. Van Schaack, Stanford Univ.*

## SUMMARY

Stacking is perhaps the most important procedure in surface seismic data processing. It is also extremely significant for crosswell reflection imaging. Big improvements in the signal-to-noise ratio of the reflection events can be achieved through appropriate use of the fold. Yet, stacking high-frequency, wide-angle reflections is not trivial. With wavelengths of a few ft, small misalignments due to velocity or geometric errors can produce destructive interference and actually degrade the events.

In this paper we present an imaging sequence that allowed us to produce high-quality stacked sections from a large cross-well dataset. A very good tie was achieved with logs recorded at both wells. Heterogeneities inside a 100-ft thick reservoir as well as dipping beds were successfully imaged, with resolution of a few ft. Imaging with these data was the computational equivalent of processing 1516 offset VSPs.

## INTRODUCTION

In recent years, several authors (Baker and Harris, 1984; Beydoun et al., 1988; Iverson, 1988; Abdalla et al., 1990; Beckey et al., 1991; Stewart and Marchisio, 1991; Lazaratos et al., 1991) advocated the use of reflections recorded in cross-well data for imaging the area between wells. For most of the real-data studies, a very small number of data gathers—or even a single gather—was used for imaging.

Compared to these previous studies, the data volume used for the work presented in this paper is enormous. As we are going to explain below, we imaged the equivalent of 1516 offset VSPs. Such a large data volume creates new domains for multichannel filtering of the cross-well data, as explained in Rector et al. (1992a) and Rector et al. (1992b). Further, it allows us to use the fold to improve the signal-to-noise ratio through stacking. Cross-well data are so complicated and rich in different modes that both improvements (better processing and stacking) are necessary to produce high-quality images. A numerical modeling analysis revealing the complexity of the cross-well data used in this study, can be found in Van Schaack et al. (1992).

In Lazaratos et al. (1991) we achieved a good tie at the well, even though we used a single gather for imaging. Yet, we were not able to reliably image away from the wells, due to poor signal-to-noise ratio. In this study, we demonstrate that, with large data volumes, appropriate processing and stacking of multiple gathers, reliable well-to-well sections can be produced from cross-well reflections.

## DESCRIPTION OF THE DATA

A description of the geology and the data acquisition is given in Harris et al. (1992).

The wavefields used for imaging were the P to P and S to S primary reflections. Unlike the direct P and S arrivals, these events are often invisible in the raw data and need to be enhanced and separated by appropriate processing. The processing sequence used for this study is discussed in detail in a companion paper (Rector et al., 1992b). As illustrated in Figure 1, for each reflection mode (P-P, S-S), we have two types of reflection wavefields: upgoing and downgoing. Upgoing reflections (reflections that are upgoing as they are received) are produced by interfaces below the source/receiver. Downgoing reflections (reflections that are downgoing as they are received) are produced by interfaces above the source/receiver. Both were used for imaging.

There is a further subdivision for every reflected wavefield (P upgoing, P downgoing, S upgoing, S downgoing). As explained in Rector et al. (1992b), it is separated, during processing, into two parts: one, sorted in common source gathers, contains reflections generated at reflection points between the receiver well and halfway the distance between wells; the other, sorted in common receiver gathers, contains reflections generated at reflection points between the source well and halfway the distance between wells. As illustrated in Figure 2, both common source and common receiver gathers go through the same imaging sequence and form two stacked sections, which are then combined to produce a final well-to-well stacked section.

This dataset consisted of 201 source and 178 receiver gathers. From each gather—common source or common receiver—we extracted four separate wavefields: P upgoing, P downgoing, S upgoing, S downgoing. So, we ended up with 804 common source gathers and 712 common receiver gathers, a total of 1516 gathers, 758 for each mode (P or S). All these gathers were taken through the imaging sequence.

## THE IMAGING SEQUENCE

The processing sequence improves the signal-to-noise ratio for the reflection events. Further improvements can be achieved by taking advantage of the data redundancy—the fold—through stacking. To effectively achieve this, one has to deal with the fact that cross-well reflection imaging is extremely sensitive to the velocity model. Some of the difficulties that we faced are similar to the difficulties associated with defining an optimal velocity model for prestack depth migration of surface seismic data. Our advantage here is that the tomogram provides a good initial velocity model. A disadvantage is that we are imaging with wide-angle reflections, whose depth positioning is more sensitive to veloc-

ity inaccuracies. In this paragraph we describe a sequence that allows us to refine our imaging operator and velocity model in a series of steps to produce a high-quality stack.

The imaging sequence flowchart is shown in Figure 3. The first step is the prestack depth imaging of the processed common source and commom receiver gathers. There are two significant issues associated with this step. The first is the choice of an appropriate velocity model. An initial model can be built based on the velocity tomogram and the sonic logs. The second is the choice of the imaging algorithm. We chose to use the VSP-CDP mapping algorithm (Wyatt and Wyatt, 1984). A brief description of our particular implementation can be found in Lazaratos et al. (1991). Although this algorithm can only handle a single dip for any particular image location, we found it to be significantly more robust than full-aperture migration algorithms, when dealing with limited-aperture noisy data.

After the data are imaged to their correct depth and horizontal location, they are sorted into common depth point (CDP) gathers. These are actually common reflection point gathers, since the ray bending effects have been accounted for at the imaging stage. If our velocity model is correct, reflection events are aligned in this domain.

We then select on each CDP gather (which corresponds to a particular horizontal location) the range of incidence angles over which the signal-to-noise ratio for the reflections is optimal. This is a significant step. It is important to avoid using extremely large angles of incidence. At these angles many of the reflections are post-critical and converted reflections (P to S, S to P) tend to be strong. Also, mapped reflections suffer from significant vertical stretch (similar to the NMO stretch) when the incidence angles are very wide. The optimal range of angles strongly depends on the signal-to-noise ratio, which in turn depends on the radiation pattern of the sources and receivers. Radiation patterns for P and S waves are different. Gathers for which the reflection point is positioned outside the optimal range of radiation angles for the particular mode, tend to contribute mostly noise rather than useful signal.

The sequence then proceeds to the first loop in the flowchart of Figure 3. The data are stacked to produce a preliminary stacked section. This section can then be used to further improve the velocity model, by allowing us to more accurately define the interfaces. It can also be used to update the imaging operator. The VSP-CDP mapping algorithm needs the reflector dip to be defined. One can start with a first estimate of the dip, produce a stacked section, then update the dip as indicated by the stack and repeat the imaging. This produces better focusing of the events whose dips were incorrectly assigned in the first pass.

The first loop (prestack imaging, CDP sorting, optimal angle range selection, stack, update imaging operator and velocity model) allows us to get a good estimate of the dominant dips and sharpen the original velocity model. Further refinement of the model can be achieved by residual velocity analysis. As mentioned before, if the velocity model is exactly correct, reflection events are aligned in CDP gathers. Curvature of the events in the CDP gathers is indicative of incorrect velocities that will produce an imperfectly focused stack. Residual velocity analysis can be used to estimate corrections to the velocity model, which will eliminate the residual curvature of the events and therefore produce a better stack. This step could be coupled with residual statics. The purpose of the statics step is to estimate and correct for abrupt changes in the traveltimes of the reflection events that cannot be explained by the velocity model, such as those produced by geometric or timing errors. Finally, the residual velocities can be used in a residual imaging step, that produces the final stacked section.

## RESULTS

The result of imaging with P to P reflections is shown in Figure 4. The velocity model used for imaging was a 1-D model derived from the tomogram shown in Harris et al. (1992). The part of the image between 1700 ft and 2000 ft was produced from downgoing reflections. The part below 2000 ft was produced from upgoing reflections. To make the two images compatible we reversed the sign of the downgoing reflections. The P-wave sonic logs and synthetics for both source and receiver wells are also shown. The synthetics shown here are just bandpass filtered versions of the logs, phase shifted by 90 degrees. The spectrum of the filter applied to the logs was an average of the spectra of our image traces.

For the result presented here, the stack was not further optimized with residual velocity analysis and statics corrections. Although overall the quality of the image is good, there are indications that it will benefit from further refinement of the velocity model. Notice, for example, that the events between 1750 and 1800 ft seem to be pulled up in the middle. The event at 2050 ft seems to be pulled down in the middle. Also some events—like the ones between 1800 and 1850 ft and the one at 1960 ft or the dipping events at the bottom of the section—are imperfectly focused.

Despite these imperfections, indicating the need for further refinements, this is a very-high-resolution, good-quality, well-to-well image. Notice the generally good tie of the section with both logs. As it is described in Harris at al. (1992), the target of this experiment was a reservoir between about 1850 and 1960 ft. Notice the large number of events between these depths, indicating heterogeneities inside the reservoir. Another interesting feature is the sequence of strong reflections between 1700 and 1800 ft. Below 2100 ft we see a sequence of dipping events. The dip correlates well with the dominant dip for this range of depths, as it is suggested by the logs. A comparison of this result to the tomogram is made in Harris at al. (1992).

## CONCLUSIONS

We proposed an imaging sequence for cross-well data and showed results from a large cross-well dataset. Imaging these data required computational effort equivalent to imaging 1516 offset VSPs.

Appropriate use of fold is a critical factor for producing high-quality well-to-well images from cross-well reflections. An optimal range of incidence angles has to be selected. Similar to prestack depth imaging of surface seismic data, the definition of a velocity model that produces a well-focused stack is extremely important. High resolution tomograms can provide good initial models. The quality of the stack can be improved through subsequent refinements of the velocity model. These refinements can be achieved by using the stacked section to better define the location of interfaces and through a residual velocity analysis step that minimizes the curvature of the reflection events in CDP gathers.

With increasing data volumes, crosswell reflection processing and imaging becomes more and more similar (in terms of computational effort) to the processing and imaging of surface seismic data, although the geometry is more similar to the VSP geometry. These large data volumes are necessary for reliable high resolution imaging of reservoirs.

## ACKNOWLEDGEMENTS

The authors would like to acknowledge the support of the Chevron Oil Field Research Company and the Gas Research Institute ( GRI ).

## REFERENCES

Abdalla, A. A., Stewart, R. R., and Henley, David, C., 1990, Traveltime Inversion and Reflection Processing of Cross-Hole Seismic Data: paper BG2.8 presented at the 1990 Annual Meeting of SEG, San Francisco, Sep.23 - 27.

Baker, L. J., and Harris, J. M., 1984, Cross-Borehole Seismic Imaging: paper BHG2.2 presented at the 1984 Annual Meeting of SEG, Atlanta, Dec.2 - 6.

Beckey, M., Bernet-Rollande, J. O., Laurent, J., and Noual, G., 1991, Imaging reflectors in a crosswell seismic experiment: paper B025 presented at the 1991 Annual Meeting of EAEG, Florence, May 26 - 30.

Beydoun, W. B., Delvaux, J., Mendes, M., Noual G., and Tarantola, A., 1988, Practical Aspects of an Elastic Migration / Inversion of Crosshole Data for Reservoir Characterization: A Paris Basin Example: Geophysics **54**, 1587 - 1595

Harris, J. M., Nolen-Hoeksema, R., Rector, J. W., Van Schaack, M., and Lazaratos, S. K., 1992, High-Resolution Cross-Well Imaging of a West Texas Carbonate Reservoir: Part 1 - Data Acquisition and Project Overview, to be presented at the 1992 Annual Meeting of SEG, New Orleans

Iverson, W. P., 1988, Crosswell Logging for Acoustic Impedance: Pet. Tech. J., 75 - 82

Lazaratos, S. K., Rector, J. W., Harris, J. M., and Van Schaack, M., 1991, High-Resolution Imaging with Cross-Well Reflection Data: paper BG4.4 presented at the 1991 Annual Meeting of SEG, Houston, Nov. 10 - 14

Rector, J. W., Lazaratos, S. K., Harris, J. M., and Van Schaack, M., 1992a, Extraction of Reflections from Cross-Well Wavefields, to be presented at the 1992 Annual Meeting of SEG, New Orleans

Rector, J. W., Lazaratos, S. K., Harris, J. M., and Van Schaack, M., 1992b, High-Resolution Cross-Well Imaging of a West Texas Carbonate Reservoir: Part 3 - Wavefield Separation, to be presented at the 1992 Annual Meeting of SEG, New Orleans

Stewart, R., R., and Marchisio, G., 1991, Cross-well Seismic Imaging Using Reflections: paper D/P1.4 presented at the 1991 Annual Meeting of SEG, Houston, Nov. 10 - 14

Van Schaack, M., Harris, J. M., Rector, J. W., and Lazaratos, S. K., 1992, High-Resolution Cross-Well Imaging of a West Texas Carbonate Reservoir: Part 2 - Wavefield Analysis and Tomography, to be presented at the 1992 Annual Meeting of SEG, New Orleans

Wyatt, K. D., and Wyatt, S. B., 1984, Determining subsurface structure using the vertical seismic profiling: In Toksoz, M. N., and Stewart, R. R., Eds, Vertical Seismic Profiling: Advanced Concepts, Geophysical Press

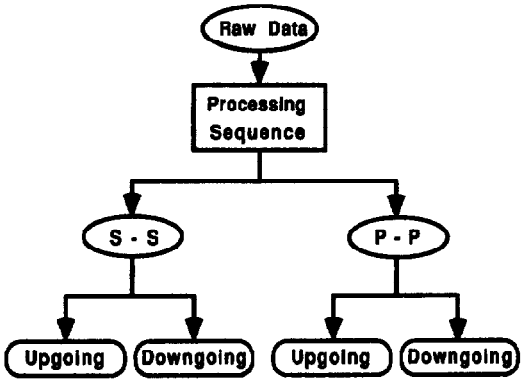


Figure 1. Wavefields used for imaging. After processing, the P to P and S to S reflections are extracted from the raw data. For each reflection mode, the data are further separated into upgoing and downgoing wavefields.

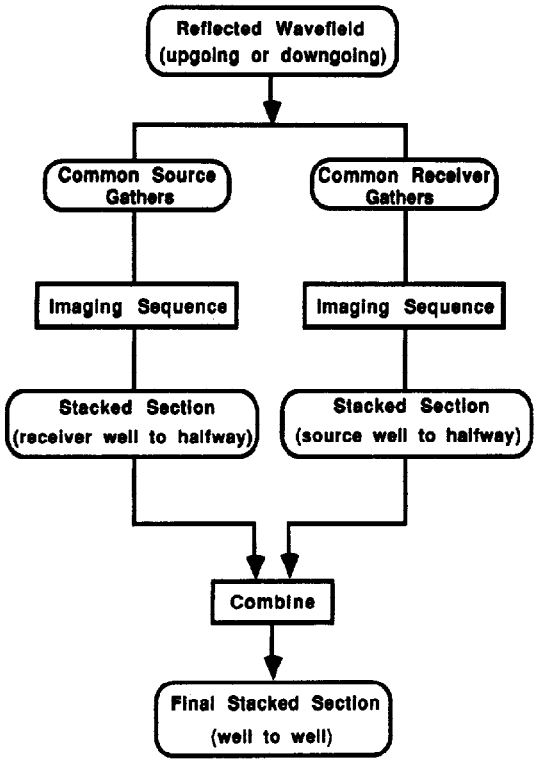


Figure 2. Flowchart showing how a reflected wavefield (upgoing or downgoing) is used for imaging. Common source and common receiver gathers are used to image different areas. The sections formed from the two different sorts are finally combined to form a well-to-well section.

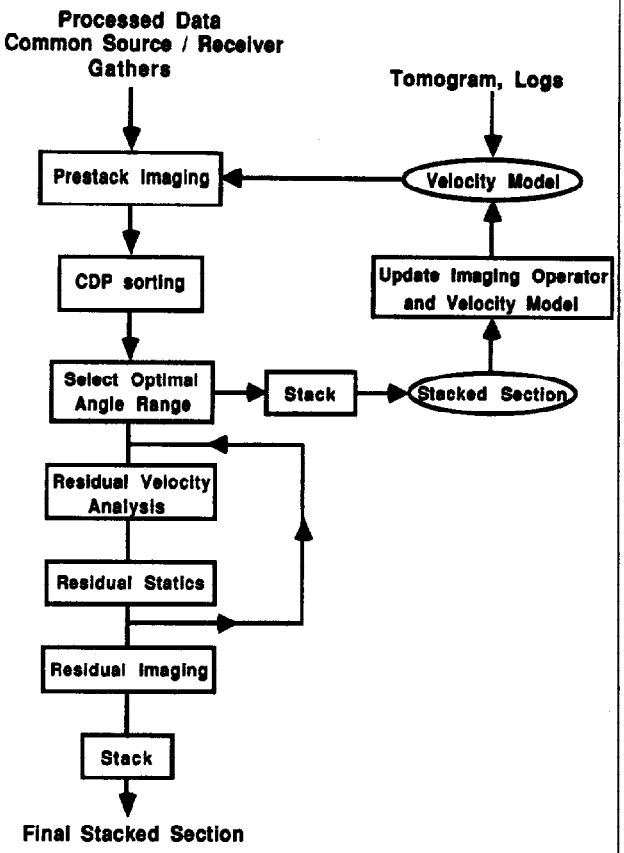


Figure 3. Flowchart for the imaging sequence. This diagram represents the interior of the "Imaging Sequence" block in Figure 2.

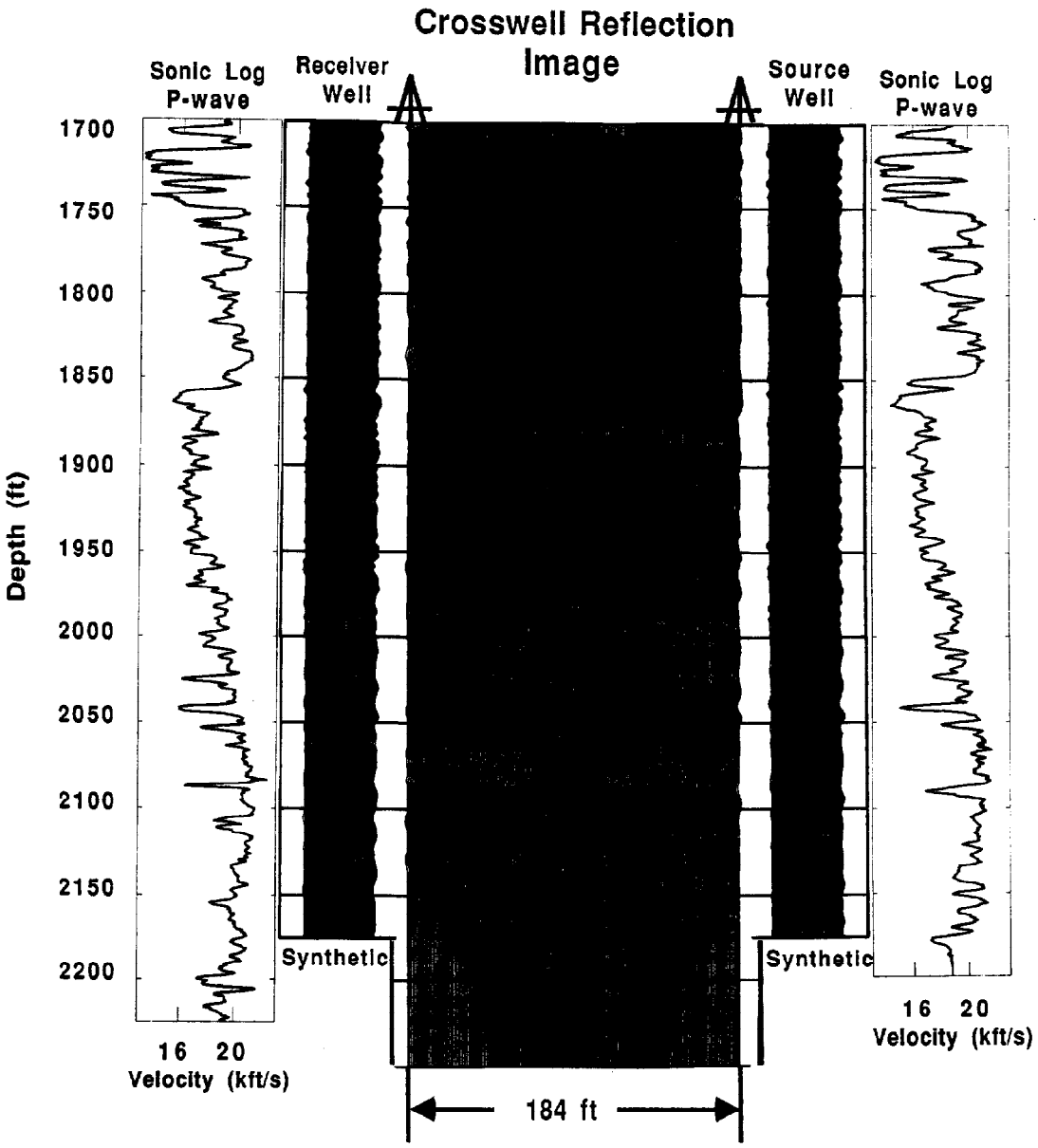


Figure 4. Result of imaging with P to P reflections. The P-wave sonic logs and synthetics for both source and receiver wells are also shown.

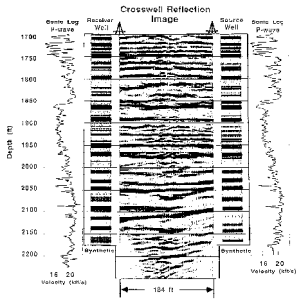
Crosswell Reflection Image
Receiver Well
Source Well
Depth (ft)
1700
1750
1800
1850
1900
1950
2000
2050
2100
2150
2200
Synthetic
Synthetic
16 20
Velocity (kft/s)
16 20
Velocity (kft/s)
184 ft